Title

Optical, structural and aging properties of Al/Sc-based multilayers for the extreme ultraviolet

Authors

Rebellato, Jennifer

Soufli, Regina

Meltchakov, Evgueni

et al.

Publication Date

2021-10-01

DOI

10.1016/j.tsf.2021.138873

Optical, structural and aging properties of Al/Sc-based multilayers for the extreme ultraviolet

Jennifer Rebellato [a,b,*], Regina Soufli [c], Evgueni Meltchakov [a], Eric M. Gullikson [d], Sébastien de Rossi [a], Cédric Baumier [e], Florian Pallier [e] and Franck Delmotte [a]

[a] *Université Paris-Saclay, Institut d'Optique Graduate School, CNRS, Laboratoire Charles Fabry, 91127, Palaiseau, France*

[b] *Centre National d'Etudes Spatiales, 18 Avenue E. Belin, 31401 Toulouse, France*

[c] *Lawrence Livermore National Laboratory, 7000 East Avenue, Livermore, California 94550, USA*

[d] *Lawrence Berkeley National Laboratory, 1 Cyclotron Rd., Berkeley, California 94720, USA*

[e] *Université Paris-Saclay, CNRS, IJCLab, 91405, Orsay, France*

Abstract

This manuscript presents the structural characterization of Al/Sc-based periodic multilayer coatings for the extreme ultraviolet (EUV) spectral range. Based on transmission electron microscopy and electron diffraction as well as grazing-incidence and large-angle x-ray diffraction, a model for the layer structure and the interfacial effects of Al/Sc coatings is built. The onset of crystallization in nanoscale Al and Sc layers as a function of thickness is also revealed in these characterizations. The Al/Sc layer model is validated and further refined by fitting in-band and out-of-band EUV reflectance measurements across 5 orders of magnitude in an extended wavelength range from 17 to 80 nm. The same type of EUV reflectance measurements is used to test the Al/Sc aging properties and to demonstrate the spectral response of optimized two- and tri-material multilayers including Al/Sc, Al/Sc/SiC and Mo/Al/Sc.

Keywords

Multilayer, aluminum, scandium, extreme ultraviolet, microstructure, synchrotron characterization

1. Introduction

Multilayer interference mirrors have become key technological components in the extreme ultraviolet (EUV) spectral range (defined as wavelengths from 10 to 80 nm). The development of multilayers with high efficiency and long-term stability has enabled several breakthroughs in science and industry in areas such as EUV lithography, solar physics, ultrafast phenomena, coherent EUV sources, etc. The long-wavelength part of the EUV spectrum remains however less explored. One major limitation in the development of multilayer coatings is the presence of interfacial effects (roughness, diffusion, interlayer formation) that are not predictable theoretically and that affect both the efficiency and the stability of the multilayer. For the experimental multilayer response to meet the design expectations, these interfacial effects need to be understood and included in the multilayer design. Thus, one needs to study in detail the physical phenomena that take place at sub-nanometric scale in any combination of multilayer materials.

Due to the presence of its L2,3 absorption edge near 17 nm, Aluminum has favorable optical properties to act as a low-absorption material in multilayer interference mirrors for

wavelengths longer than the L2,3 edge. Aluminum-based multilayers for the EUV have been extensively studied over these last ten years [1–3] and Al/Mo/SiC multilayer coatings have been developed and deposited on Solar Obiter EUV telescopes [4].

Sc has been proposed as an efficient low-absorption material for EUV radiation above the Sc M2,3 absorption edge (about 44 nm) [5] and Sc/Si multilayers with near normal incidence reflectance as high as 56.6% at 44.7 nm have been developed [6].

We have recently proposed to combine Al and Sc in the same multilayer [7,8] and we have demonstrated experimentally Al/Sc-based multilayers with high reflectance at wavelengths longer than the Sc M3 edge (up to 57.5% at 44.7 nm and 46.5% at 51 nm). Actually, simulations show that Al/Sc multilayer mirrors can provide high normal-incidence reflectance on a very broad spectral range, from 17 nm to beyond 60 nm (see Figure 1). Moreover, the addition of a third material (such as SiC or Mo) in the periodic structure produces even higher reflectance values.

In this paper, we present the analysis of the microstructure, aging properties and in-band and out-of-band EUV response of periodic Al/Sc multilayers with various layer thicknesses ranging from 5 nm to 20 nm. Transmission Electron Microscopy (TEM) and electron diffraction, as well as Large-Angle X-ray Diffraction (LAXRD) and grazing incidence X-Ray Reflectometry (XRR), provided detailed information about the layer and interface structure. The near-normal incidence EUV reflectance of these samples was measured across 5 orders of magnitude on a broad spectral range (17 nm to 80 nm). Based on the structural analysis results, a model is proposed and is further refined by fitting the EUV reflectance data. The lifetime stability of these Al/Sc samples is also studied via EUV reflectance measurements. Finally, we used these results to develop two- and tri-material Al/Sc-based multilayers (Al/Sc, Al/Sc/SiC and Mo/Al/Sc) with optimized reflectance in the EUV range 44 - 60 nm.

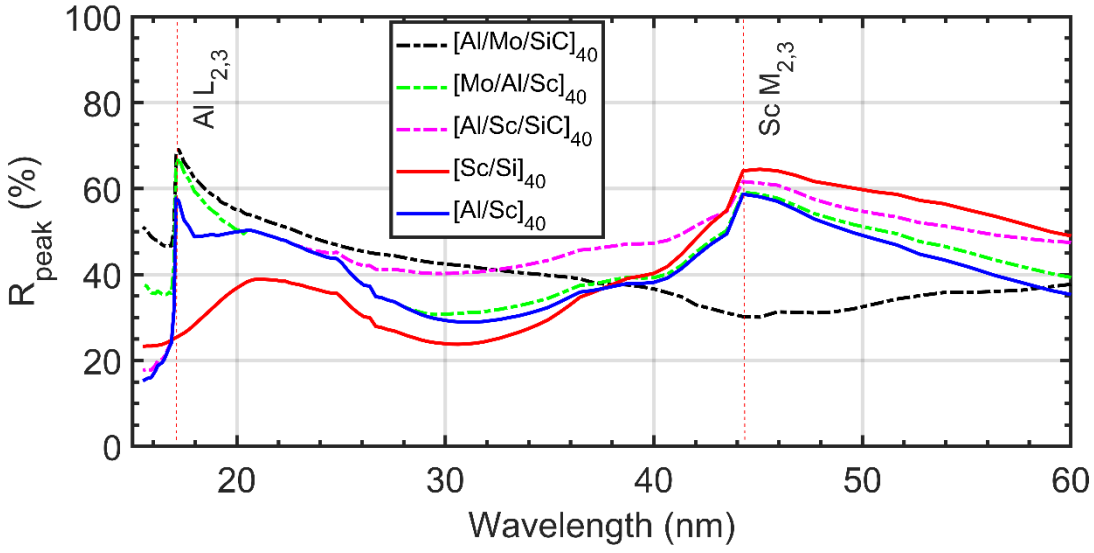

Figure 1. Calculated, ideal (zero interfacial roughness, no capping layer) peak reflectance (R_{peak}) is plotted vs. wavelength for Sc/Si, Al/Sc, Al/Sc/SiC, and Mo/Al/Sc multilayers at normal incidence. The number of periods in each multilayer has been chosen in order to saturate the peak reflectance in the entire wavelength range and is shown in the legend as a subscript.

2. Experimental details

2.1. Selection of multilayer structures

As shown in Figure 1, the calculated ideal maximum reflectance values were obtained with a code written in Matlab© using optical constants from Aquila et al. [9] for wavelength below 25 nm and from Uspenskii et al. [5] for wavelength above 25 nm for Sc, Palik et al. [10] for Al and Mo, and Kortright and Windt [11] for SiC. These optical constant values have been selected and evaluated in earlier work [12,13], and represent the available values from the literature that provide the best agreement to experimental reflectance measured on multilayers deposited in our machine. Notice that evaporated Sc optical constants published by Fernández-Perea et al. [14] give also good results. Nevertheless, we chose optical constants from Uspenskii et al. [5] which are measured on sputtered Sc (same deposition technique as in this study) and which give slightly better agreement in the absorption edge region (see [13], Fig. 61 on p.83). These optical constants will be also used for the fitting models presented in subsections 3.2.1 and 3.3.2. In the Matlab code used in Fig. 1, the algorithm finds for each photon energy the optimal thicknesses that satisfy the Bragg condition to within 10% by taking an average index of the two or three materials. Then, the algorithm uses an optimization method based in the interior-point technique, with constraint to find the thicknesses which minimize the reflectivity deviation to one. The constraint imposes a positive thickness, smaller than the wavelength.

Because the microstructure properties of layers and interfaces in a multilayer are often dependent on the thickness of each constituent layer, a set of Al/Sc samples was prepared with different layer thicknesses, to study these thickness-dependent effects. The layer thickness range (5 nm to 20 nm) is representative of the thicknesses needed to realize multilayer coatings in the EUV. Table 1 shows the design (goal) layer values for the Al/Sc multilayers prepared for the layer thickness study (labeled as "Thickness study samples") discussed in Sections 3.1 and 3.2, as well as for the optimized multilayers (labeled "Optimized samples") that are discussed later in Section 3.3.

2.2. Fabrication and Characterization techniques

All multilayers were prepared at *Laboratoire Charles Fabry* with a magnetron sputtering system, which can accommodate up to four targets and can be used either in a Radio Frequency (RF) or a Direct Current (DC) mode according to the deposited material [15]. The substrates were Si wafer pieces in (100) crystal orientation with surface microroughness in the 0.2 nm range. We used Mo, SiC and Sc targets and a Si-doped (1.5 wt. %) Al target, with better than 99.95% purity. During the deposition process, we used a 2.7×10^{-1} Pa Ar pressure in the deposition chamber. The plasma discharge was established with a DC current of 0.1 A for the Sc target, 0.06 A for the Mo target, and a RF power of 200 W and 150 W for the Al and SiC targets, respectively. We protected all the "thickness study" samples with a 3 nm thick SiC top layer. We have previously demonstrated that such SiC capping layers are able to assure a good temporal stability of Al-based multilayers [16,17]. For the optimized samples, we adjusted the SiC top layer thickness in order to reach the highest reflectance (see Table 1).

All samples were measured by XRR at 8.05 keV (Cu Kα line, $\lambda = 0.154$ nm) on a Bruker Discover D8™ diffractometer. Fits to the XRR data have been completed with the commercial Leptos © software in order to determine the multilayer period, layer thickness and average values of layer interface roughness/diffusion. For the modelling at 8.05 keV, we

used optical constants from the Henke tables [18] with the tabulated densities of 3.16 g/cm^3 for SiC, 3.00 g/cm^3 for Sc, 2.70 g/cm^3 for Al, 10.22 g/cm^3 for Mo and 2.33 g/cm^3 for Si, respectively. We have also performed LAXRD experiments for a few samples in Bragg-Brentano geometry using a Panalytical Empyrean™ system with a front focusing mirror for the Cu Kα radiation (λ = 0.154 nm) and a PIXcel -3D detector.

Table 1. Goal values of layer thicknesses (d_{Al}, d_{Sc}, $d_{SiC\ (Mo)}$, d_{Top}) and multilayer period thicknesses (D_{ML}) for Al/Sc thickness study samples, and Al/Sc, Al/Sc/SiC and Mo/Al/Sc optimized samples. d_{Top} represents the thickness of the top SiC layer (capping layer). In the second column, the number of bilayers in each sample is shown as a subscript and the SiC capping layer is shown as a separate layer, when it is not part of the periodic structure. All thickness and roughness values are indicated in nanometers.

#	Multilayer structure	d_{Al}	d_{Sc}	$d_{SiC\ (Mo)}$	d_{Top}	D_{ML}
		Thickness study samples				
8026	$[Al/Sc]_{40}$ / SiC	5	5	--	3	10
8028	$[Al/Sc]_{10}$ / SiC	10	10	--	3	20
8030	$[Al/Sc]_{10}$ / SiC	20	20	--	3	40
8031	$[Sc/Al]_{10}$ / SiC	10	10	--	3	20
8032	$[Al/Sc]_{10}$ / SiC	5	20	--	3	25
8033	$[Al/Sc]_{10}$ / SiC	20	5	--	3	25
		Optimized samples				
9049	$[Al/Sc/SiC]_{20}$	10.18	9.71	4.17	--	24.06
9051	$[Mo/Al/Sc]_{20}$ / SiC	8.04	11.60	4.47	5	24.11
9052	$[Mo/Al/Sc]_{7}$ / SiC	11.1	16.89	8.16	10	36.15
9055	$[Al/Sc]_{25}$ / SiC	13.97	9.5	--	5	23.47
9056	$[Al/Sc]_{25}$ / SiC	16.45	12.47	--	5	28.92
9060	$[Al/Sc/SiC]_{20}$	11.97	12.11	5.68	--	29.76

The EUV reflectance measurements discussed in Sections 3.2 and 3.3.2 were performed at beamline 6.3.2. of the Advanced Light Source (ALS) synchrotron at LBNL. Beamline 6.3.2. has a grating monochromator with a fixed exit slit and its general characteristics have been described in detail earlier [19,20]. A set of filters of various materials (with each filter selected specifically for each wavelength range) is used for wavelength calibration and 2nd harmonic and stray light suppression. For higher-order harmonic suppression, an "order suppressor" consisting of three mirrors at a variable incidence angle (depending on wavelength range) and based on the principle of total external reflection is used in addition to the filters. In this manuscript, measurements were performed with the 80 lines / mm monochromator grating and with the order suppressor consisting of 3 Carbon mirrors at 20 degrees grazing incidence angle. An Al filter (17.5 – 25.5 nm) and a Mg filter (25 – 50 nm) were used for 2nd harmonic and stray light suppression, while no filter was used at 45 – 80 nm. Wavelength was calibrated based on the $L_{2,3}$ absorption edge of an Al filter and the wavelength accuracy was 5×10^{-3} nm.

The beamline 6.3.2. measurement chamber allows translation of the sample in three dimensions, tilt in two dimensions and azimuth rotation of the sample holder. The available detectors include various photodiodes and a CCD camera (the latter for sample alignment), which can be rotated by 360° around the axis of the chamber. During the measurements discussed in this manuscript, signal was collected with a Si photodiode detector with a 10×10 mm^2 active area and acceptance angle of 2.4°. The ALS storage ring current was used to normalize the signal, and the reflectance accuracy was 0.1% (absolute). The base pressure in the measurement chamber was 10^{-5} Pa. All samples were stored in a clean environment and measured two to four weeks after deposition.

Results shown in section 3.1.2. were obtained using a transmission electron microscope FEI: TECNAI G² 20 Twin at the *Centre de Sciences Nucléaires et de Sciences de la Matière (CSNSM)* belonging to the JANNUs platform. It is equipped with a LaB_6 electron gun and operates under a vacuum of 8.10^{-6} Pa with a 200 kV voltage. This microscope can reach a spatial resolution of 0.27 nm with a minimum spot size of 10 nm at 200 kV. The electron transparency of the analyzed Al/Sc multilayer sample has been reached thanks to a flat-type tripod polishing technique. For this, the flat-type polished specimen mounted on a tripod was thinned down using diamond lapping films according to the procedure described in Cha et al. [21]. The last step of the procedure required to use a GATAN PIPS I ion milling machine exposing the specimen to two asymmetric ion beams of Ar^+ in grazing incidence to ensure the electron transparency of the sample. The analyzed Al/Sc 8028 multilayer sample

was fabricated in October 2018 and the TEM preparation and measurements were realized a few months later. We used this TEM microscope in imaging and electron diffraction modes.

3. Results and discussion

3.1. Microstructure analysis of Al/Sc multilayer coatings

3.1.1. XRR measurements at 8.05 keV

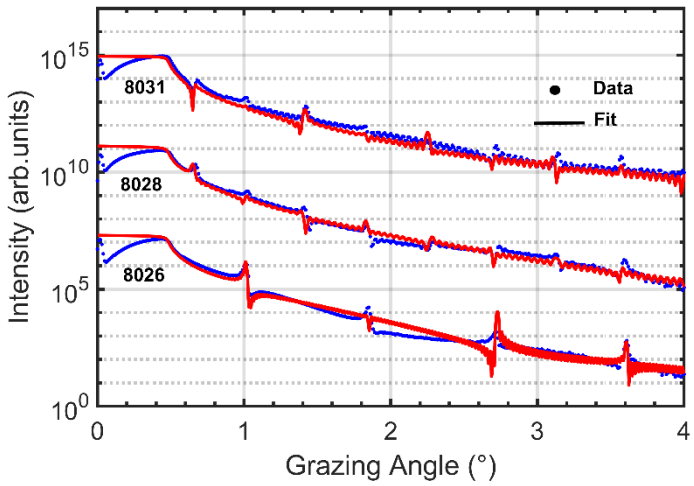

Figure 2. XRR-measured (blue data points) and fitted (red solid lines) curves at 8.05 keV for Al/Sc 8026, 8028 and 8031 multilayer samples.

All Al/Sc multilayers labeled "Thickness study samples" (see Table 1) were measured by grazing incidence XRR at 8.05 keV. The fitted layer thickness and roughness values are summarized in Table 2. The XRR measurements and fits for Al/Sc samples 8026, 8028 and 8031 are shown in Figure 2. The fit sensitivity is estimated to be 0.01 nm for the period thickness and close to 0.1 nm for the individual layer thicknesses. The low optical contrast between Al and Sc at 8.05 keV [18] does not allow pronounced peaks in the XRR data. However, the good agreement between simulated and experimental intensities of the successive Bragg peaks indicates good layer quality and periodicity for all three samples. The fitted interfacial roughness/diffusion values were between 0.5 and 0.7 nm (Table 2).

3.1.2. Transmission Electron Microscopy: imaging and electron diffraction of Al/Sc samples

As the reflectivity of multilayer mirrors in the EUV can strongly depend on the crystallinity properties of their layer structure and most crucially on the quality of the interfaces between each layer of material, we employed TEM to characterize the structural features of one of the Al/Sc multilayers, sample 8028. The as-designed thicknesses of Al and Sc layers are 10 nm, near the middle of the thickness range of this study. In Figure 3, we show TEM bright field images of the 8028 Al/Sc sample. In Figure 3 (a), aluminum and scandium layers are clearly distinguishable, with aluminum layers appearing darker than scandium. Also, Al columnar structures appear textured, while Sc layers appear mostly amorphous. Some dark spots randomly appearing in the Sc layers of the multilayer are suspected to be due to the last sample preparation step of ion milling, during which some clusters of atoms are pulled off the layers. Figure 3 (b) is a detail on the selected area of Figure 3 (a). We have determined the grey level profile (green solid line) by an integration on the horizontal axis over the entire selected

area. The results clearly indicate the existence of an Al-Sc interlayer (IL) between each Al and Sc layer, with an average thickness of about 3 nm.

Table 2. XRR-fitted layer thicknesses ($d_{Al\ XRR}$, $d_{Sc\ XRR}$, $d_{Top\ XRR}$), multilayer period thicknesses ($D_{ML\ XRR}$) and interfacial roughness/diffusion values ($\sigma_{Al\ XRR}$, $\sigma_{Sc\ XRR}$, $\sigma_{Top\ XRR}$) for Al/Sc thickness study multilayer samples. d_{Top} represents the thickness of the top SiC layer (capping layer). In the second column, the number of bilayers in each sample is shown as a subscript and the SiC capping layer is shown as a separate layer. All thickness and roughness values are indicated in nanometers.

#	Multilayer structure	$d_{Al\ XRR}$	$d_{Sc\ XRR}$	$d_{Top\ XRR}$	$D_{ML\ XRR}$	$\sigma_{Al\ XRR}$	$\sigma_{Sc\ XRR}$	$\sigma_{Top\ XRR}$
8026	$[Al/Sc]_{40}$ / SiC	4.92	4.95	3.02	9.87	0.77	0.50	0.58
8028	$[Al/Sc]_{10}$ / SiC	9.94	10.00	3.02	19.94	0.74	0.45	0.61
8030	$[Al/Sc]_{10}$ / SiC	20.04	19.88	3.02	39.92	0.70	0.53	0.58
8031	$[Sc/Al]_{10}$ / SiC	9.76	10.19	3.09	19.95	0.63	0.51	0.44
8032	$[Al/Sc]_{10}$ / SiC	5.18	19.42	3.01	24.60	0.71	0.55	0.69
8033	$[Al/Sc]_{10}$ / SiC	20.87	4.21	2.97	25.07	0.72	0.45	0.55

The electron diffraction mode of the microscope allowed us to quantitatively characterize the crystallization features of the 8028 Al/Sc sample.

In the electron diffraction images (Figure 4 (a) & (b)), the central spot is the direct electron beam, the bright spots around it are associated to crystalline orientations, and diffuse circles are characteristic of amorphous phases. For a polycrystalline phase, spots appear along a thin circle at the same distance from the central spot.

The measured distance between the central spot and the spot of interest is then a 1/nm value that can be used to determine the interplanar distance (d_{hkl}) of the associated crystal. Based on this principle and appropriate comparisons with diffraction databases [22], we started the analysis by identifying the crystalline orientations for the (100) silicon substrate (not explicitly shown here) as a reference for the identifications associated with the multilayer materials.

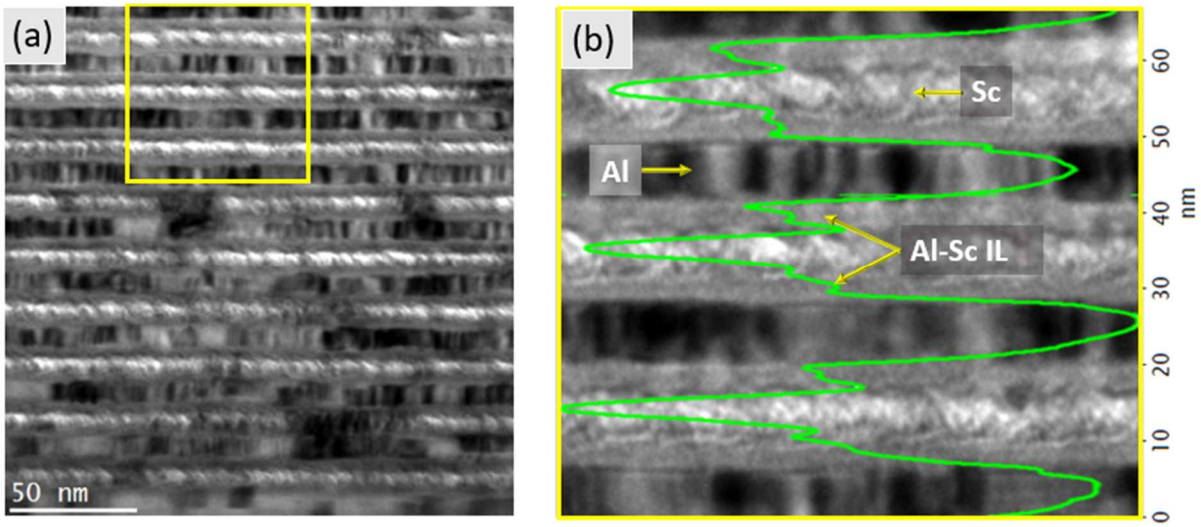

Figure 3. Bright field TEM images of the 8028 [Al/Sc]x10 sample prepared with mechanical flat-type tripod polishing. (a) is a x50k image and (b) is a x100k image of the selected area shown in (a), showing in detail the Al and Sc layers and Al-Sc interlayers (IL).

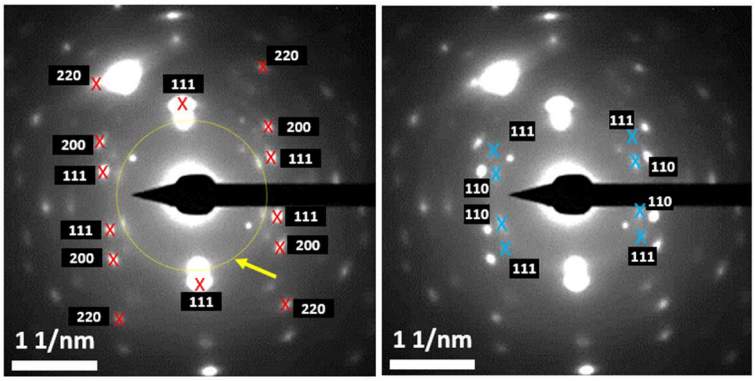

Figure 4. 8028 Al/Sc multilayer electron diffraction images with identification of crystalline orientations for Al (a) and Al_3Sc (b). Scandium layers are amorphous and appear as a diffuse circle as indicated on (a).

We have determined (111), (200) and (220) crystalline orientations for aluminum with $d_{(111)}$ = 2.329 Å (theoretical value = 2.329 Å), $d_{(200)}$ = 2.024 Å (theoretical value = 2.031 Å), and $d_{(220)}$ = 1.431 Å (theoretical value = 1.459 Å). This is in good agreement with the columnar structures appearing in the bright field images (Figure 3 (a) & (b)). A diffuse circle on the electron diffraction diagram stands for the amorphous state of scandium (Figure 4 (a)). Also, features linked to the Al_3Sc alloy in Figure 4 (b) have been identified as (111) and (110) orientations with $d_{(111)}$= 2.368 Å (theoretical value = 2.368 Å) and $d_{(110)}$=2.900 Å (theoretical value = 2.885 Å), respectively. Al_3Sc could be one of the main components of the interlayers seen in the TEM bright field images (Figure 3 (a) & (b)).

3.1.3. Large Angle X-ray Diffraction results for Al/Sc multilayer coatings

We characterized the 8032 (Al 5.18 nm / Sc 19.42 nm) and 8033 (Al 20.87 nm / Sc 4.21 nm) samples by LAXRD, because their thickness asymmetry could be interesting towards revealing specific thickness-dependent crystallinity properties of Al, Sc and Al-Sc alloy.

In Figure 5, we can identify the characteristic peak of the (400) reflection associated to the Si (100) oriented substrate at 69.15° along with its forbidden reflection line (200) at 33° for both samples. The occurrence of the forbidden reflection line (200) is caused by multiple diffraction as demonstrated in Zaumseil et al. [23]. In the LAXRD data of the 8033 Al/Sc sample containing more Al than Sc, we are noticing pronounced Al peaks, Al (111) at 38.5° and Al (222) at 83.3°, but no significant scandium crystallization is detected, as is discussed below.

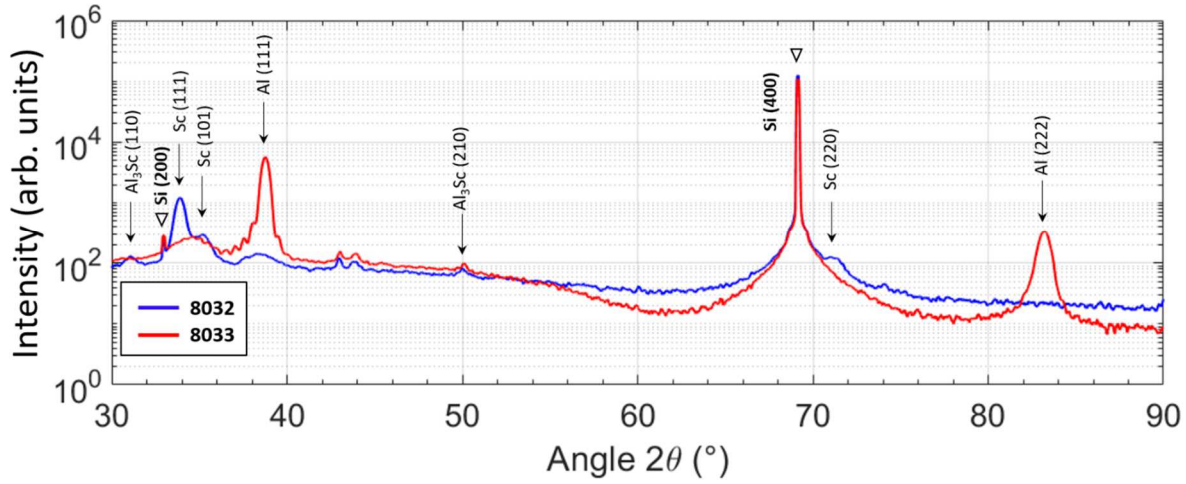

Figure 5. Large Angle X-Ray Diffraction analysis of 8032 and 8033 Al/Sc multilayer samples.

On the other hand, the 8032 Al/Sc sample which contains more Sc than Al, presents three Sc reflections: Sc (111) at 33.9°, Sc (101) at 35°, and Sc (220) at 70.94° next to the main Si (400) peak. We can suggest that the weak and wide signal observed in the 8032 data around the Al (111) position is associated to a polycrystalline phase of aluminum. The same characteristic is observed for scandium in the 8033 data around the Sc (111) and (101) positions. On both sets of data, we have determined at least one orientation due to the Al_3Sc alloy: Al_3Sc (110) and (210) for the 8032 sample, and (210) only for the 8033 sample. We can add that two diffraction peaks have been observed on every sample diffractogram at 42° and 45° (not annotated). However, their identification remains unclear despite our research in the literature but as they systematically show the same relative intensity, we can infer that they are not associated with the Al or Sc layers. Further studies would be needed to solve this question.

In order to calculate the average crystallite size, *L*, from the LAXRD Al (111) and Sc (111) peaks, we used the Scherrer formula [24]:

$$L = \frac{K \times \lambda}{FWHM \times cos\theta}$$

where λ is the X-ray wavelength in nanometers, FWHM is the Full Width at Half Maximum of the diffraction peak in radians, θ is the Bragg angle and K is a constant related to crystallite shape usually taken as 0.89 [25]. According to this equation, one finds an average crystallite size of about 17.8 nm from the Al (111) peak of the 8033 multilayer sample and an average crystallite size of about 12 nm from the Sc (111) peak of the 8032 multilayer sample. These values are consistent with the Al and Sc layer thickness in each sample and confirm that the 20 nm Al layers are more strongly crystallized than the Sc ones. Similar values for magnetron sputtered Al have been reported in previous work [26,27].

It is demonstrated from TEM images, electron diffraction and LAXRD analysis that the Al_3Sc phase appears in all Al/Sc multilayer samples, indicating that this alloy is one of the components of the Al-Sc interlayer. Also, for Al layer thicknesses greater than 5 nm, we notice an obvious Al crystallization according to the (111) direction, which appears as columnar structures in the bright-field TEM images. Sc crystallization was identified on LAXRD data for the 8032 sample only, containing Sc layers of about 20 nm. Given that no crystalline phases of Sc were found in the TEM and electron diffraction analysis of sample 8028 with 10 nm-thick Sc layers (Section 3.1.2), it is concluded that Sc layers thicker than 10 nm seem to be necessary to initiate the crystallization of Sc.

3.2. Reflectometry results in the EUV for "thickness study" Al/Sc samples

3.2.1. Reflectance measurements in the EUV for Al/Sc multilayers

We have measured the performance of the Al/Sc "thickness study samples" (see Table 1) in the EUV at the ALS synchrotron over a wide wavelength range that covers multiple Bragg order reflection peaks. To fit the EUV data, we propose fitting models according to the structural information obtained from XRR, TEM, electron diffraction and LAXRD analyses. We remind that the "thickness study samples" discussed in this Section were not optimized in layer thickness to reach specific reflectance or peak wavelength. The experimental results are summarized in Table 3 for the 8026, 8028, 8030, 8031 and 8033 Al/Sc samples, and the measured EUV data and models are shown in linear and logarithmic scale in Figure 6 (a) & (b), (samples 8028 and 8031) and Figure 7 (a) & (b) (samples 8026 and 8033).

Table 3. Experimental values of EUV peak reflectance (R_{exp} in %), peak wavelength (λ_{exp} in nm) and bandwidth (BW_{exp} in nm) for Al/Sc samples

#	Multilayer structure	R_{exp} (%)	λ_{exp} (nm)	BW_{exp} (nm)
8026	$[Al/Sc]_{40}$ / SiC	34.1	19.1	0.65
8028	$[Al/Sc]_{10}$ / SiC	28.4	39.3	5.9
8030	$[Al/Sc]_{10}$ / SiC	27.2	60.6	5.2
8031	$[Sc/Al]_{10}$ / SiC	17.6	42.1	7.65
8033	$[Al/Sc]_{10}$ / SiC	36.9	44.3	2.95
		21.6	24.2	1.15

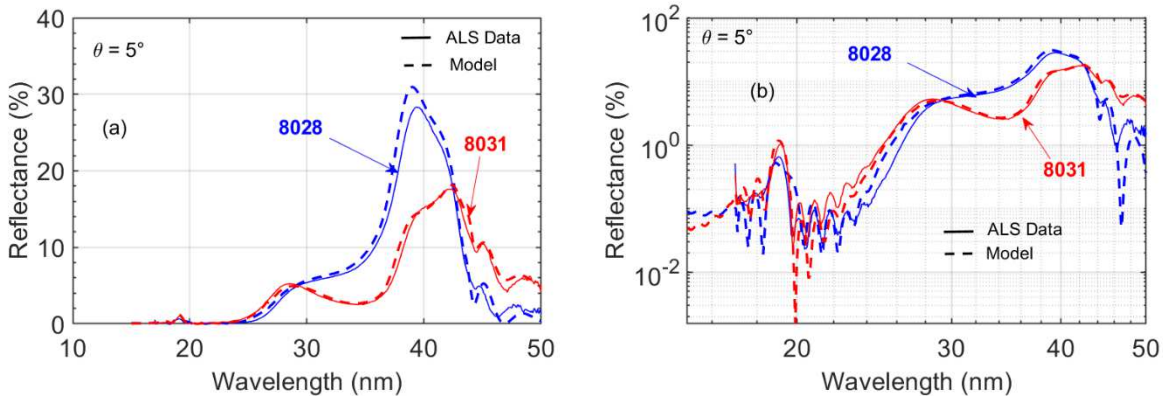

Figure 6. Measured and fitted reflectance vs. wavelength data for the 8028 (Al/Sc) and 8031 (Sc/Al) samples near normal incidence (θ = 5°) in linear (a) and logarithmic scale (b). The 2nd order multilayer Bragg peak is visible near 19 nm wavelength, in (b).

Comparison between the 8028 and 8031 EUV reflectance data (Figure 6) is of great interest as the two samples only differ by the deposition order of the Al and Sc layers, with Al being the first layer deposited on the Si substrate for sample 8028 and Sc being the first layer deposited on the Si substrate for sample 8031. We notice that the 8031 $[Sc/Al]_{10}$ multilayer presents a peak reflectivity of 17.6% at 42.1 nm, while the 8028 $[Al/Sc]_{10}$ reaches 28.4% at 39.3 nm. Their bandwidths are 5.9 nm and 7.65 nm for 8028 and 8031, respectively. This significant difference in peak reflectance and bandwidth values is well reproduced with simulation and can be explained by the position of the maxima and minima of the electric field standing wave within the multilayer structure and at the top surface of the multilayer. If we compare the electric field intensity of each sample at their peak wavelength (Figure 7), one can observe that the electric field intensity is close to its maximum (standing wave anti-node) within the 3 nm thick SiC capping layer for the 8031 $[Sc/Al]_{10}$ sample, while it is close to its minimum (standing wave node) for the 8028 $[Al/Sc]_{10}$ sample. Hence, the reflectivity is strongly reduced for the 8031 multilayer sample compared to the 8028 sample. These results show that the order of deposition can have a dramatic influence on the performance of the multilayer in this wavelength range. Moreover, it suggests that the optimization of the thickness of the top layer could improve the reflectivity of the multilayer samples as we will see in the next Section. Similar effects have been reported for the optimization of Mo/Si and Sc/Si multilayer structures by [28] [29].

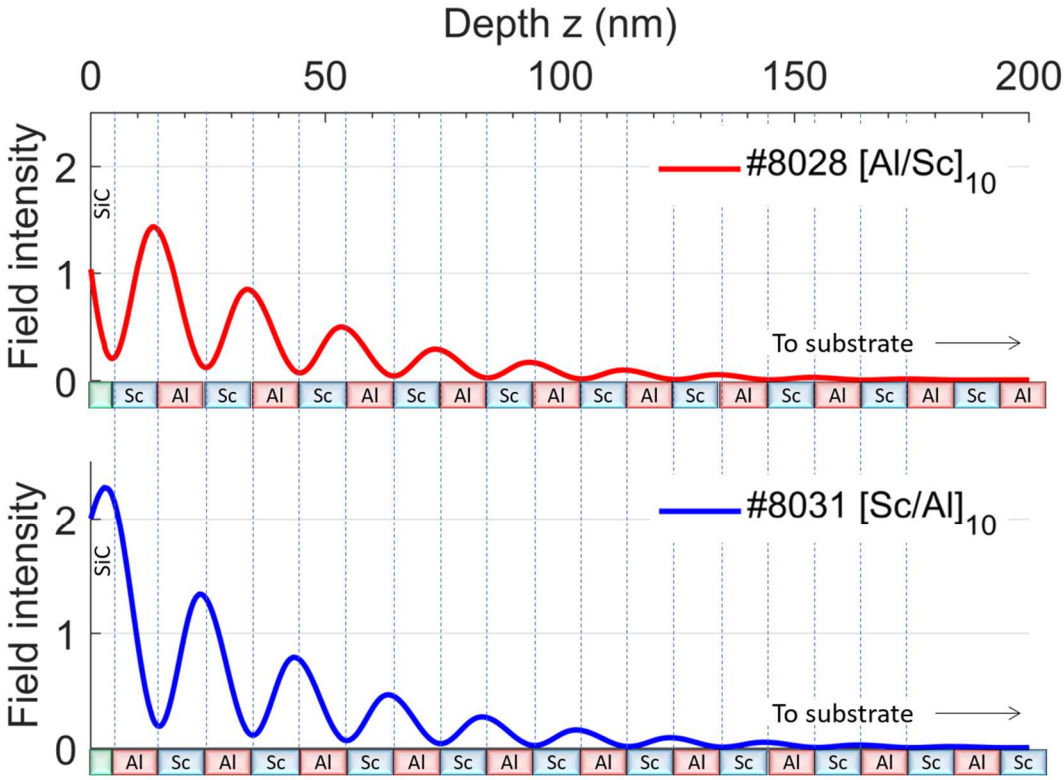

Figure 7. Effect of deposition order and top (capping) layer on the intensity of the electric field in $[Al/Sc]_{10}$ 8028 and $[Sc/Al]_{10}$ 8031 multilayer coatings.

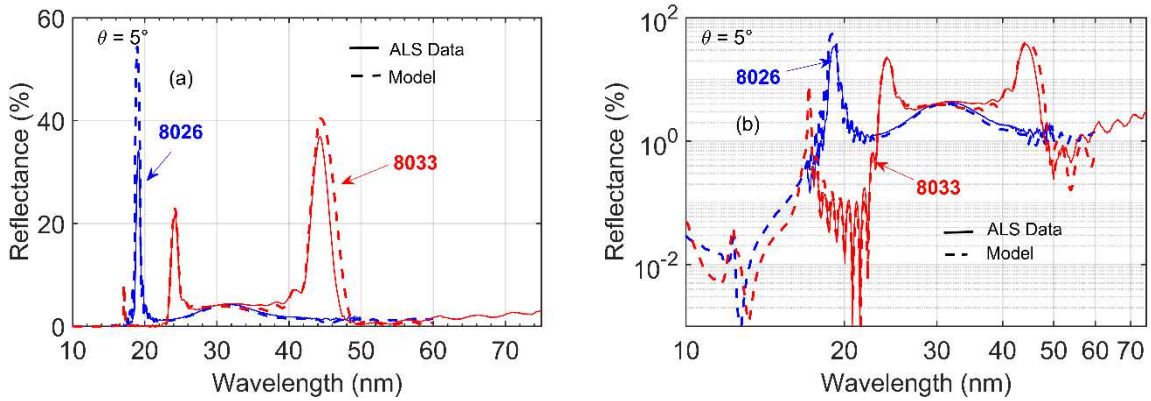

Figure 8. Measured and fitted data for the 8026 and 8033 Al/Sc samples near normal incidence (θ=5°) in linear (a) and logarithmic scale (b).

The EUV reflectance data and models for samples 8026 and 8033 are shown in (Figure 8 and Table 3): sample 8026 reaches 34.1% reflectance at 19.1 nm with a 0.65 nm bandwidth, and the 8033 sample presents a reflectance peak of 36.9% at 44.3 nm with the 2nd order Bragg peak of about 22% at 25 nm.

The fitting models to the EUV data for samples 8026, 8028, 8031 and 8033 are based on the fits of XRR data : we used the period thickness and roughness values given in Table 2. All models include a native SiO_2 oxide layer of about 1-1.5 nm on top of the SiC capping layer, which is presumably formed after exposure of these coatings to air. In a first attempt, we tried to fit the EUV experimental data with a 2-layer (Al/Sc) model similar to the XRR model. However, the fits (not shown here) were not satisfactory. Consequently, based on the

structural results reported in the previous section, we included interfacial layers at Sc-on-Al and/or Al-on-Sc interfaces in the fitting models. These interfacial layers were implemented using the "graded interface" function of the IMD software [30] and we adjusted their position within the multilayer stack in order to obtain the best fit to the EUV data. As a result, the Al and Sc layer thicknesses decrease in order to keep the Al/Sc bilayer period thickness constant. The thicknesses of each layer used in the models corresponding to these fits, including Al-on-Sc and Sc-on-Al interfacial layers, are shown in Table 4. Note that the optical constants of the interface layers are calculated directly by taking the average of the optical constants of the surrounding layers.

Due to the significant uncertainties of available optical constant values for Sc and Al above 40 nm wavelengths and around absorption edges, we chose to focus the fits in the spectral range below 40 nm. As shown in Figure 6 and Figure 8, we were able to accurately fit the detailed features of the EUV reflectance measurements below 40 nm. The inclusion of the interfacial layers was crucial in achieving the high quality of the fits.

Table 4. Layer thicknesses of the models used to fit XRR (d) and EUV (d') reflectance of samples 8026, 8028, 8031 and 8033.

	XRR model		EUV model			
#	d (Al) (nm)	d (Sc) (nm)	d'(Al) (nm)	d'(Sc) (nm)	Sc-on-Al interlayer (nm)	Al-on-Sc interlayer (nm)
8026	4.92	4.95	4.68	4.50	0.7	None
8028	9.94	10.0	7.96	5.98	3.0	3.0
8031	9.76	10.19	9.11	8.68	1.1	1.1
8033	20.87	4.21	19.0	3.59	2.5	None

The values of layer thicknesses for the 8028 sample are consistent with the TEM observations in Figure 3. Concerning the 8026 and 8033 multilayers, we have reached the best agreement between EUV reflectance data and fits by adding only one interfacial layer, at the Sc-on-Al interface. It should be noted that both 8026 and 8033 contain thinner Sc layers (5 nm) than 8028 and 8031 (10 nm) in their structures. The thickness of the interfacial layer seems to be correlated to the thickness of the deposited layers, which is why the simulated 8026 interface is only 0.7 nm in width (both Al and Sc layers in sample 8026 are about 5 nm in thickness). As the 8031 sample is the only one to be deposited with an inverted order of layers, we cannot firmly explain so far why 1.1 nm thick interlayers are sufficient to obtain the fitting model as we expected 3 nm thick interlayers based on the 8028 sample. However, despite this difference in thickness that would deserve to be studied further, adding interfacial layers in the model improved the fits to the EUV measurements, for all samples.

This method gave good results for Al/Sc multilayer samples across the EUV range, despite uncertainties in the optical constant values around absorption edges and above 40 nm wavelength in the spectral range. Any discrepancies between the measured data and fits above 40 nm on Figure 6 and Figure 8 are representative of the uncertainties in the EUV optical constant values.

3.2.2. Aging effects on the performance of Al/Sc multilayers

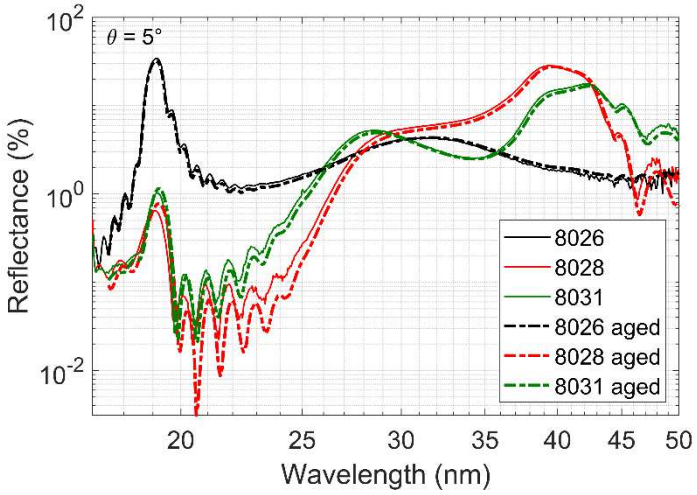

Figure 9. Reflectance vs. wavelength measurements (plotted in log-log axes) of 8026, 8028 and 8031 Al/Sc multilayer samples in November 2018 and in August 2019.

Nine months after the first EUV measurements shown in Figs. 6 and 8, we have measured again the EUV reflectance of samples 8026, 8028 and 8031 at ALS beamline 6.3.2, to determine their temporal stability. During the time in-between measurements, the samples were kept in laboratory ambient conditions. Figure 9 clearly shows the good stability of Al/Sc multilayer structures: we notice good agreement in all characteristic features, including Bragg 1st and 2nd order and Kiessig fringes. This good structural stability has also been confirmed by XRR measurements (not shown here). It turns out that 8026 reached 31.9% reflectance at 19.1 nm (-2.2% absolute), 8028 reached 27.6% at 39.7 nm (-0.8%) and 8031 showed a reflectance of 16.6% at 42.4 nm (-1.0%). These changes are in the typical range of EUV coating evolution in the first year after deposition [16] and may be explained by a modification of the top layer (oxidization and/or contamination) [17]. These results demonstrate adequate temporal stability of the EUV performance of Al/Sc multilayers protected with a 3 nm thick SiC capping layer.

3.3. Optimization of two- and tri-material Al/Sc-based multilayers in the EUV range

3.3.1. XRR measurements at 8.05 keV

The promising XRR and EUV reflectance results obtained with the Al/Sc "thickness study samples" and the data gathered through the structural analyses discussed in the previous Section were used to design and deposit two- and tri-material Al/Sc-based multilayers with optimized reflectance at near-normal incidence, at EUV wavelengths longer than 40 nm. The samples were measured by XRR at 8.05 keV. The layer parameters fitted from the XRR data are shown in Table 5. Plots of the XRR data and fits of three samples are shown as examples in Figure 10.

As shown in Figure 10, the good agreement between simulated and experimental intensities of the successive Bragg peaks indicates good layer quality and periodicity for all samples. The fitted interfacial roughness/diffusion values were between 0.5 and 0.7 nm. Also, we note that adding a third material (Mo or SiC) in the Al/Sc structures allowed to reach a stronger optical contrast at 8.05 keV, resulting in more distinct Bragg peaks, compared to those in Fig. 2.

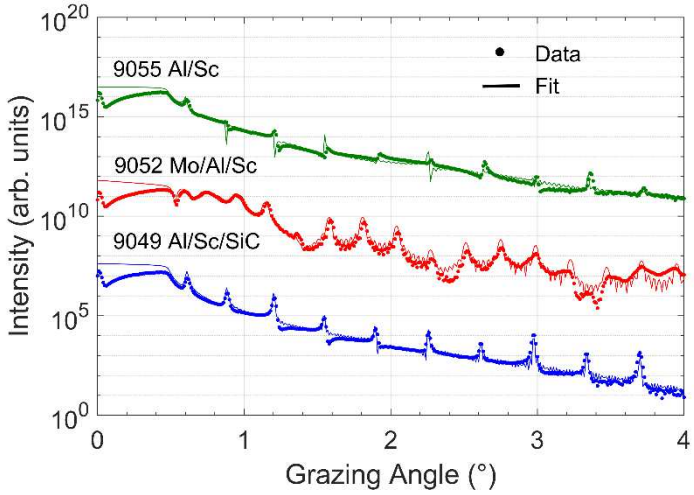

Figure 10. XRR measured (dots) and fitted (solid lines) curves at 8.05 keV for 9049, 9052 and 9055 multilayer samples.

Table 5. XRR-fitted layer thicknesses ($d_{Al\ XRR}$, $d_{Sc\ XRR}$, $d_{SiC\ (Mo)\ XRR}$, $d_{Top\ XRR}$), multilayer period thicknesses ($D_{ML\ XRR}$) for optimized Al/Sc-based multilayer samples. d_{Top} represents the thickness of the top SiC layer (capping layer). In the second column, the number of bilayers in each sample is shown as a subscript and the SiC capping layer is shown as a separate layer. All thickness values are indicated in nanometers.

#	Multilayer structure	$d_{Al\ XRR}$	$d_{Sc\ XRR}$	$d_{SiC\ (Mo)\ XRR}$	$d_{Top\ XRR}$	$D_{ML\ XRR}$
8030*	$[Al/Sc]_{10}$ / SiC	20.04	19.88	--	3.02	39.92
9049	$[Al/Sc/SiC]_{20}$	10.18	9.71	4.17	--	24.06
9051	$[Mo/Al/Sc]_{20}$ / SiC	7.92	11.40	4.56	5.05	23.87
9052	$[Mo/Al/Sc]_{7}$ / SiC	11.32	16.72	8.13	9.73	36.17
9055	$[Al/Sc]_{25}$ / SiC	14.30	9.70	--	5.23	23.90
9056	$[Al/Sc]_{25}$ / SiC	16.00	13.50	--	5.00	29.51
9060	$[Al/Sc/SiC]_{20}$	11.97	12.11	5.68	--	29.76

3.3.2. Reflectance measurements of optimized multilayers in the EUV: Al/Sc, Al/Sc/SiC and Mo/Al/Sc

The Al/Sc-based, optimized multilayer samples were measured in a wide wavelength range from about 17 nm to 80 nm at ALS beamline 6.3.2. shortly after their fabrication. In a former work [8], we reported on the record peak reflectance of these coatings but we only focused in a limited spectral range around the 1st Bragg reflectance peaks. Here, we present extended-wavelength EUV data for Al/Sc, Al/Sc/SiC and Mo/Al/Sc multilayer samples with their fitted values based on graded interface models discussed in Section 3.2.1. The EUV results of the optimized Al/Sc-based samples are summarized in Table 6.

Table 6. Experimental values of EUV peak reflectance (R_{exp} in %), peak wavelength (λ_{exp} in nm) and bandwidth (BW_{exp} in nm) for optimized Al/Sc-based multilayer coatings.

#	Multilayer structure	R_{exp} (%)	λ_{exp} (nm)	BW_{exp} (nm)
9049	$[Al/Sc/SiC]_{20}$ / SiC	56.5	44.7	4.2
9051	$[Mo/Al/Sc]_{20}$ / SiC	48.1	45.2	4.6
9052	$[Mo/Al/Sc]_{7}$ / SiC	37.4	57.3	11.2
9055	$[Al/Sc]_{25}$ / SiC	55.9	44.7	3.6

9056	$[Al/Sc]_{25}$ / SiC	42.4	51	4.1
9060	$[Al/Sc/SiC]_{20}$ / SiC	46.5	51	5.6

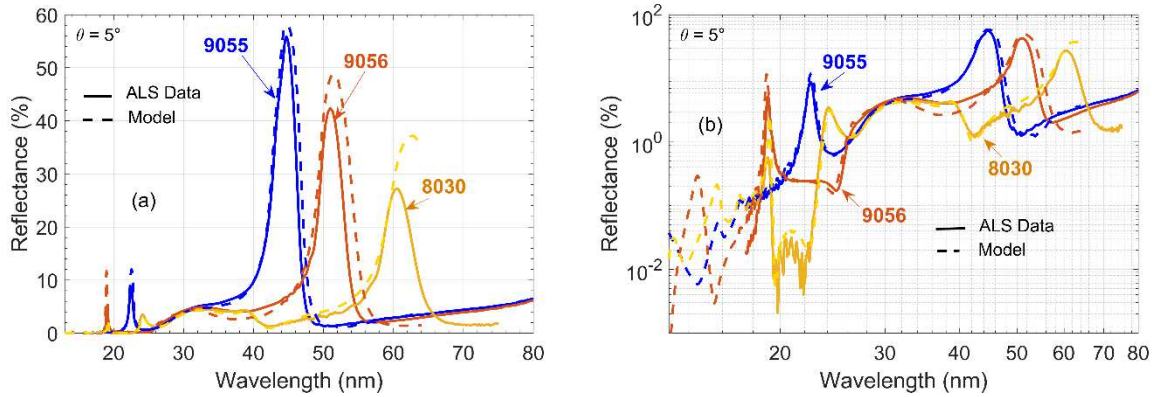

Figure 11. Measured (solid line) and fitted (dash line) reflectance vs. wavelength values for optimized Al/Sc multilayers in the EUV in linear scale (a) and logarithmic scale (b).

In Figure 11 (a), it is interesting to observe that optimized periodic Al/Sc multilayer mirrors reach a peak reflectivity of 55.9 % at 44.7 nm wavelength close to the Sc $M_{2,3}$ absorption edge, and then their peak reflectance decreases for longer wavelengths. However, all samples maintain a 3.5 nm to 4.1 nm peak bandwidth which are good selectivity values in this spectral range. Also, in Figure 11 (b) we can see the complex fine structure associated with the 1st and 2nd order Bragg peaks as well as fine structure in-between peaks, for each Al/Sc sample. These features served as a reference in the fitting process of the interfacial layers resulting in accurate fits in an extended wavelength range, over 5 orders of magnitude in reflectance values. As in the previous sections, period thickness and roughness values deduced from XRR data were used and a 1-1.5 nm SiO_2 native top oxide layer was added in the fits. The thicknesses and position of Al-on-Sc and Sc-on-Al interfacial layers were adjusted in order to fit the EUV data. For all these samples, we have been able to obtain good fits by adding only a 2 nm thick Sc-on-Al interfacial layer (Table 7).

Table 7. Layer thicknesses of the models used to fit the EUV reflectance data from 8030, 9055, and 9056 Al/Sc samples.

	XRR model		EUV model			
#	d (Al) (nm)	d (Sc) (nm)	d' (Al) (nm)	d' (Sc) (nm)	Al-on-Sc interlayer (nm)	Sc-on-Al interlayer (nm)
8030	20.0	19.9	19.6	18.3	None	2.0
9055	14.3	9.7	13.9	8.1	None	2.0
9056	16.0	13.5	15.6	11.9	None	2.0

Optimized Al/Sc/SiC periodic multilayer mirrors reached 56.5% and 46.5% peak reflectivity near the Sc absorption edge (Figure 12). At 44.7 nm, the 9049 Al/Sc/SiC sample reached a better reflectance (+0.6%) than the 9055 Al/Sc, as well as a slightly wider spectral bandwidth (+0.6 nm). Further from the Sc absorption edge, the improvement in reflectance values of Al/Sc/SiC compared to Al/Sc is more pronounced (as is expected in 3-material vs. 2-material systems) as the 9060 Al/Sc/SiC sample reaches 46.5% at 51 nm vs. a 42.4% reflectance value at 51 nm for 9056 Al/Sc.

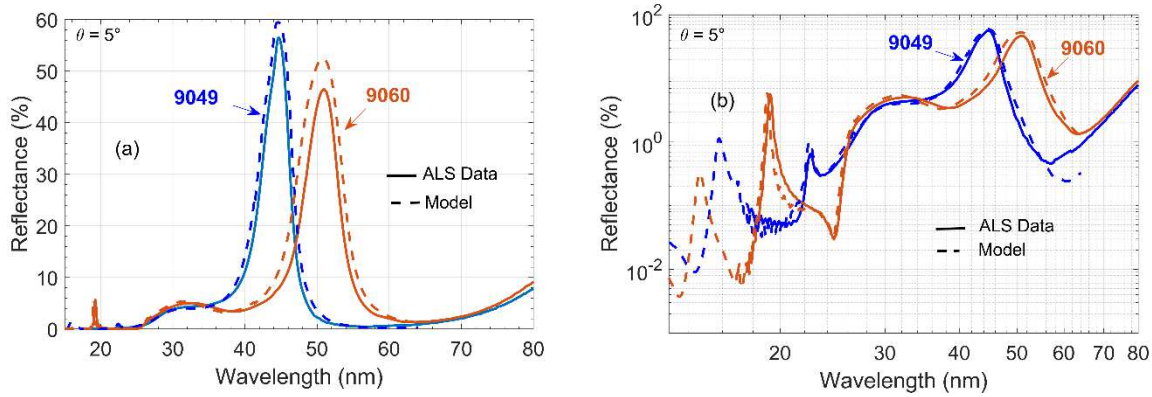

Figure 12. Measured (solid line) and fitted (dash line) reflectance vs. wavelength values for optimized Al/Sc/SiC multilayers in the EUV in linear scale (a) and logarithmic scale (b).

In Figure 12 (b), we observe fine structures related to higher order Bragg peaks for wavelengths between 17 nm and 30 nm. As previously, these data were used as a reference for the fitting process. Unlike Al/Sc multilayer samples, we only have a Sc-on-Al interface in this Al/Sc/SiC configuration, and no Al-on-Sc interface. Therefore, after adding an oxide layer we had to adjust the Sc-on-Al graded interface thickness and position (Table 8) to obtain the fitted data shown on Figure 12 (a) & (b). The results obtained with a 2 nm thick Sc-on-Al graded interface in both samples were sufficiently coherent with the data, providing an indication that the SiC-on-Sc and Al-on-SiC interfaces are sharper than the Sc-on-Al ones, and do not involve an interlayer of appreciable thickness. So, we chose to avoid SiC-on-Sc and Al-on-SiC graded interface modelling estimations.

Table 8. Layer thicknesses of the models used to fit EUV reflectance of Al/Sc/SiC 9049 and 9060 samples. The SiC-on-Sc and Al-on-SiC interfacial layers were not included in the model.

	XRR model		EUV model		
#	d (Al) (nm)	d (Sc) (nm)	d' (Al) (nm)	d' (Sc) (nm)	Sc-on-Al interlayer (nm)
9049	10.2	9.7	9.8	8.1	2.0
9060	12.0	12.1	11.6	10.5	2.0

In Figure 13, Mo/Al/Sc multilayer samples show interesting reflectance and bandwidth values above 40 nm wavelength especially near 60 nm where the 9052 sample reaches 37.4% at 57.3 nm with a wide bandwidth of 11.2 nm. Al/Sc multilayer samples reached lower reflectance values in this range (Figure 11). Mo optical constant sets are significantly limited in this spectral range and they contain some unreliable values, thus preventing the development of accurate models [12]. Despite these optical constant uncertainties, we have obtained satisfactory fits to the EUV data and the fitted layer thicknesses are shown in Table 9.

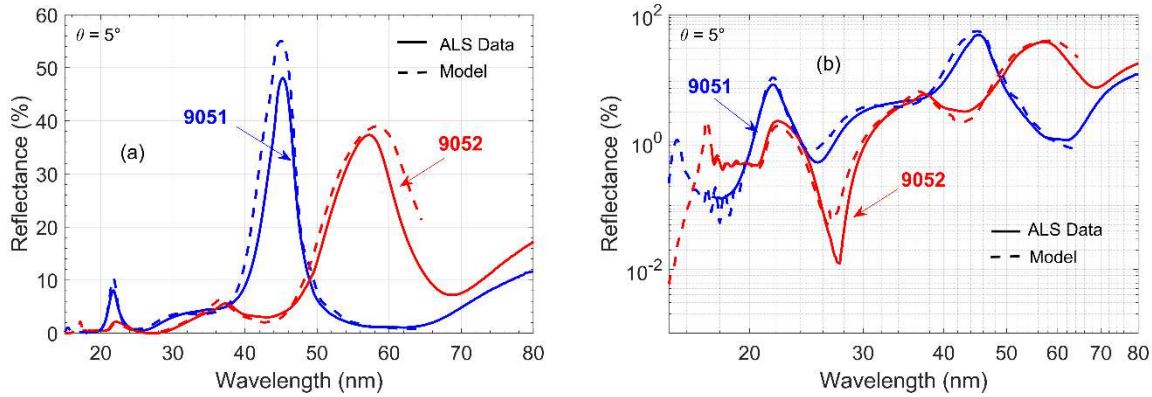

Figure 13. Measured (solid line) and fitted (dash line) reflectance vs. wavelength values for optimized Mo/Al/Sc multilayers in the EUV in linear scale (a) and logarithmic scale (b).

Table 9. Layer thicknesses of the models used to fit the EUV reflectance of 9051 and 9052 Mo/Al/Sc samples. A Mo-on-Sc interfacial layer was not included in the model.

	XRR model			EUV model				
#	d(Al) (nm)	d(Sc) (nm)	d(Mo) (nm)	d'(Al) (nm)	d'(Sc) (nm)	d'(Mo) (nm)	Al-on-Mo interlayer (nm)	Sc-on-Al interlayer (nm)
9051	7.92	11.4	4.56	6.73	9.6	2.25	3.3	2.0
9052	11.32	16.72	8.13	8.88	14.92	6.97	3.4	2.0

4. Conclusions

Motivated by encouraging simulations and initial data indicating high reflectance values in the EUV range, we have developed a series of Al/Sc multilayer coatings in order to study their microstructure. We followed by fabricating optimized Al/Sc-based multilayer coatings to reach high efficiencies in the EUV at near-normal incidence, mainly above 40 nm wavelengths. The analyses of Al/Sc samples by XRR, TEM, electron diffraction and LAXRD revealed the crystallization properties of Al and Sc layers, with crystallization initiated by a minimum layer thickness of 5 nm for Al and 10 nm for Sc. The presence of an interlayer is revealed at the Al-on-Sc and Sc-on-Al interfaces, ranging from 1 to 3 nm in thickness, depending on the thicknesses of the Al and Sc layers. Moreover, the Al_3Sc phase was identified as one of the components of the Al-Sc interlayer.

Experimental EUV reflectance results of optimized Al/Sc-based multilayer coatings (Al/Sc, Al/Sc/SiC and Mo/Al/Sc) included peak reflectivities in the range 27.2% - 56.5% at wavelengths in the range 44.7-60.6 nm, along with bandwidth values ranging from 3.5 to 11.2 nm. The results of the microstructural analyses were then included in the modeling of in-band and out-of-band EUV reflectance data performed over an extended range of wavelengths from 17 nm to 80 nm for Al/Sc, Al/Sc/SiC and Mo/Al/Sc multilayer coatings. These results allowed the refinement of fitting models, reaching a close agreement with the EUV measurements over 5 orders of magnitude, despite persistent uncertainties in the optical constant values available in the literature. A second set of EUV measurements on three Al/Sc samples 9 months later, demonstrated adequate temporal stability of the EUV performance of Al/Sc multilayers protected with a 3 nm thick SiC capping layer.

The results presented in this paper will enable the development of instrumentation in a wavelength range that has not been widely accessible up until now. Narrowband, dual band, or broadband mirrors with high peak reflectance can be achieved in the wavelength range 44 nm – 60 nm by using Al/Sc, Al/Sc/SiC and/or Mo/Al/Sc multilayers. They will address applications including coherent light sources (synchrotrons, free-electron lasers, EUV lasers, high-harmonic generation), attosecond physics, as well as solar, plasma and planetary physics.

Acknowledgements

All multilayer samples have been deposited as part of CeMOX (Couches minces pour l'Optique X), a platform of Laboratoire Charles Fabry. This work was performed under the auspices of the U.S. Department of Energy by Lawrence Livermore National Laboratory (LLNL) under Contract No. DE-AC52-07NA27344, and by the University of California Lawrence Berkeley National Laboratory under Contract No. DE-AC03-76F00098. Funding was provided by the Jean d'Alembert fellowship program from Université Paris-Saclay and LLNL's Professional Research and Teaching leave program.

References

[1] E. Meltchakov, C. Hecquet, M. Roulliay, S. Rossi, Y. Menesguen, A. Jérome, F. Bridou, F. Varniere, M.-F. Ravet-Krill, F. Delmotte, Development of Al-based multilayer optics for EUV, Appl. Phys. A. 98 (2010) 111–117. https://doi.org/10.1007/s00339-009-5445-2.

[2] D.L. Windt, J.A. Bellotti, Performance, structure, and stability of SiC/Al multilayer films for extreme ultraviolet applications, Appl. Opt. 48 (2009) 4932–4941.

[3] Q. Zhong, W. Li, Z. Zhang, J. Zhu, Q. Huang, H. Li, Z. Wang, P. Jonnard, K. Le Guen, J.-M. André, Optical and structural performance of the Al (1% wtSi)/Zr reflection multilayers in the 17–19nm region, Opt. Express. 20 (2012) 10692–10700.

[4] P. Rochus, F. Auchere, D. Berghmans, E. Al, The Solar Orbiter EUI instrument: The Extreme Ultraviolet Imager, Astron. Astrophys. (2020). https://doi.org/10.1051/0004-6361/201936663.

[5] Y.A. Uspenskii, J.F. Seely, N.L. Popov, A.V. Vinogradov, Y.P. Pershin, V.V. Kondratenko, Efficient method for the determination of extreme-ultraviolet optical constants in reactive materials: application to scandium and titanium, JOSA A. 21 (2004) 298–305.

[6] S.A. Yulin, F. Schaefers, T. Feigl, N. Kaiser, Enhanced reflectivity and stability of Sc/Si multilayers, in: Adv. Mirror Technol. X-Ray EUV Lithogr. Laser Appl., International Society for Optics and Photonics, 2004: pp. 155–164. https://doi.org/10.1117/12.505582.

[7] F. Delmotte, M. Dehlinger, C. Bourassin-Bouchet, S. de Rossi, A. Jerome, E. Meltchakov, F. Varnière, Multilayer optics for coherent EUV/X-ray laser sources, in: X-Ray Lasers Coherent X-Ray Sources Dev. Appl. XI, International Society for Optics and Photonics, 2015: p. 958907. https://doi.org/10.1117/12.2188048.

[8] J. Rebellato, R. Soufli, E. Meltchakov, E. Gullikson, S. de Rossi, F. Delmotte, High efficiency Al/Sc-based multilayer coatings in the EUV wavelength range above 40 nanometers, Opt. Lett. 45 (2020) 869. https://doi.org/10.1364/OL.384734.

[9] A.L. Aquila, F. Salmassi, E.M. Gullikson, F. Eriksson, J. Birch, Measurements of the optical constants of scandium in the 50-1300eV range, in: R. Soufli, J.F. Seely (Eds.), Denver, CO, 2004: p. 64. https://doi.org/10.1117/12.563615.

[10] E.D. Palik, ed., Handbook of optical constants of solids, 6. Nachdr., Acad. Press, Orlando, 1985.

[11] J.B. Kortright, D.L. Windt, Amorphous silicon carbide coatings for extreme ultraviolet optics, Appl. Opt. 27 (1988) 2841–2846.
[12] J. Rebellato, S. de Rossi, X. Zhang, F. Auchère, E. Meltchakov, F. Delmotte, R. Soufli, Analyses of tabulated optical constants for thin films in the EUV range and application to solar physics multilayer coatings, in: M. Lequime, H.A. Macleod, D. Ristau (Eds.), Proc SPIE Adv. Opt. Thin Films VI, SPIE, Frankfurt, Germany, 2018: p. 106911U. https://doi.org/10.1117/12.2313346.
[13] J. Rebellato, Miroirs interférentiels efficaces dans l'extrême ultraviolet pour la physique solaire, PhD Thesis, Université Paris-Saclay, 2020. https://pastel.archives-ouvertes.fr/tel-03165571
[14] M. Fernández-Perea, J.I. Larruquert, J.A. Aznárez, J.A. Méndez, L. Poletto, A.M. Malvezzi, A. Giglia, S. Nannarone, Determination of optical constants of scandium films in the 20-1000 eV range, J. Opt. Soc. Am. A. 23 (2006) 2880. https://doi.org/10.1364/JOSAA.23.002880.
[15] J. Gautier, F. Delmotte, M. Roulliay, F. Bridou, M.-F. Ravet, A. Jérome, Study of normal incidence of three-component multilayer mirrors in the range 20–40 nm, Appl. Opt. 44 (2005) 384–390.
[16] E. Meltchakov, S. De Rossi, R. Mercier, F. Varniere, A. Jérome, F. Auchere, X. Zhang, M. Roulliay, F. Delmotte, Single and multi-channel Al-based multilayer systems for space applications in EUV range, in: Damage VUV EUV X-Ray Opt. IV EUV X-Ray Opt. Synergy Lab. Space III, International Society for Optics and Photonics, 2013: p. 87771C.
[17] F. Delmotte, E. Meltchakov, S. de Rossi, F. Bridou, A. Jérome, F. Varnière, R. Mercier, F. Auchère, X. Zhang, B. Borgo, C. Dumesnil, S. François, M. Roulliay, U. Strauch, Development of multilayer coatings for solar orbiter EUV imaging telescopes, in: S. Fineschi, J. Fennelly (Eds.), Proc SPIE Sol. Phys. Space Weather Instrum. V, SPIE, San Diego, United States, 2013: p. 88620A. https://doi.org/10.1117/12.2036050.
[18] B.L. Henke, E.M. Gullikson, J.C. Davis, X-ray interactions: photoabsorption, scattering, transmission, and reflection at E=50-30000 eV, Z=1-92, Atomic Data and Nuclear Data Tables Vol.54 (no.2), 181-342 (July 1993); henke.lbl.gov/optical_constants/
[19] J.H. Underwood, E.M. Gullikson, High-resolution, high-flux, user friendly VLS beamline at the ALS for the 50–1300eV energy region, J. Electron Spectrosc. Relat. Phenom. 92 (1998) 265–272. https://doi.org/10.1016/S0368-2048(98)00134-0.
[20] E.M. Gullikson, S. Mrowka, B.B. Kaufmann, Recent developments in EUV reflectometry at the Advanced Light Source, in: Emerg. Lithogr. Technol. V, International Society for Optics and Photonics, 2001: pp. 363–373. https://doi.org/10.1117/12.436712.
[21] H.-W. Cha, M.-C. Kang, K. Shin, C.-W. Yang, Transmission Electron Microscopy Specimen Preparation of Delicate Materials Using Tripod Polisher, Appl. Microsc. 46 (2016) 110–115. https://doi.org/10.9729/AM.2016.46.2.110.
[22] S. Gates-Rector, T. Blanton, The Powder Diffraction File: a quality materials characterization database, Powder Diffr. 34 (2019) 352–360. https://doi.org/10.1017/S0885715619000812.
[23] P. Zaumseil, High-resolution characterization of the forbidden Si 200 and Si 222 reflections, J. Appl. Crystallogr. 48 (2015) 528–532. https://doi.org/10.1107/S1600576715004732.
[24] P. Scherrer, Estimation of the size and internal structure of colloidal particles by means of röntgen, Nachr Ges Wiss Gött. 2 (1918) 96–100.
[25] J.I. Langford, A.J.C. Wilson, Scherrer after sixty years: A survey and some new results in the determination of crystallite size, J. Appl. Crystallogr. 11 (1978) 102–113. https://doi.org/10.1107/S0021889878012844.
[26] S. Taheriniya, S.S. Parhizgar, A.H. Sari, Investigating the effect of sputtering conditions on the physical properties of aluminum thin film and the resulting alumina template, Results Phys. 9 (2018) 1428–1435. https://doi.org/10.1016/j.rinp.2018.03.060.
[27] R. Soufli, M. Fernández-Perea, S.L. Baker, J.C. Robinson, J. Alameda, C.C. Walton, Spontaneously intermixed Al-Mg barriers enable corrosion-resistant Mg/SiC multilayer coatings, Appl. Phys. Lett. 101 (2012) 043111. https://doi.org/10.1063/1.4737649.
[28] J. Gautier, F. Delmotte, F. Bridou, M.F. Ravet, F. Varniere, M. Roulliay, A. Jerome, I. Vickridge, Characterization and optimization of magnetron sputtered Sc/Si multilayers for extreme ultraviolet optics, Appl. Phys. A. 88 (2007) 719–725. https://doi.org/10.1007/s00339-007-4041-6.

[29] M. Singh, J.J.M. Braat, Capping layers for extreme-ultraviolet multilayer interference coatings, Opt. Lett. 26 (2001) 259. https://doi.org/10.1364/OL.26.000259.
[30] D.L. Windt, IMD—Software for modeling the optical properties of multilayer films, Comput. Phys. 12 (1998) 360. https://doi.org/10.1063/1.168689.